Waste Management 227 (2027) 115865

Contents lists available at ScienceDirect

Waste Management

journal homepage: www.elsevier.com/locate/wasman

Research Paper

High-temperature treatment and partial vitrification of fine-grained municipal solid waste incineration bottom ash: Mineralogical and chemical behaviour and reuse potential

Luciana Mantovani [a,*], Sabrina Nazzareni [a], Andrea Bernasconi [b], Enrico Destefanis [b], Caterina Caviglia [b], Chiara De Matteis [a], Valerio Funari [c,e], Simone Toller [c], Laura Fornasini [d], Danilo Bersani [d], Mario Tribaudino [b]

[a] Dipartimento di Scienze Chimiche, della Vita e della Sostenibilità Ambientale, Università di Parma, Plesso Scienze della Terra, Parco Area delle Scienze 157/A, 43124 Parma, Italy
[b] Dipartimento di Scienze della Terra, Università degli Studi di Torino, Via Valperga Caluso 35, 10125 Torino, Italy
[c] CNR-ISMAR Istituto di Scienze Marine del Consiglio Nazionale delle Ricerche, Bologna, Italy
[d] Dipartimento di Scienze Matematiche, Fisiche e Informatiche, Università di Parma, Unità di Fisica, Parco Area delle Scienze 7/A, 43124 Parma, Italy
[e] CNR - ISMN Istituto per lo Studio dei Materiali Nanostrutturati, Via Gobetti 101, Bologna, Italy

ARTICLE INFO

Keywords:
Municipal solid waste incineration bottom ash (MSWI-BA)
Thermal treatments
Vitrification
Raman spectroscopy
Chemical leaching
Glass-ceramics
Secondary raw materials

ABSTRACT

Finest grain-size fractions of municipal solid waste incineration bottom ash (MSWI-BA) represent a critical barrier to ash valorisation because they are commonly enriched in soluble salts and potentially toxic elements. This study evaluates whether thermal treatment can reduce the short-term leachability and improve the reuse potential of fine-grained MSWI-BA from the Parma Waste-to-Energy (WtE) plant by linking mineralogical and microstructural evolution to EN 12457–2 batch-leaching behaviour. The 0–2 mm fraction and selected finer sub-fractions were thermally treated at selected temperatures up to 1200 °C and characterised by XRF, ICP-MS, XRD with quantitative phase analysis, Raman spectroscopy, SEM-EDS, and leaching tests. The untreated ash consists mainly of an amorphous/glassy aluminosilicate matrix with secondary carbonates, hydrates, and sulfate- and chloride-bearing phases, whereas the finest fractions show higher concentrations of alkalis, soluble salts, and other minor phases bearing potentially ecotoxic elements. Thermal treatment causes progressive dehydration, decarbonation, recrystallization and, above approximately 1000 °C, the formation of a Ca-silicate glass–ceramic assemblage containing pyroxene and wollastonite. Above approximately 1050–1100 °C, the amorphous fraction increases again, indicating partial vitrification. This evolution is accompanied by a marked decrease in electrical conductivity and in the release of chloride, sulfate, alkalis, and several regulated elements. Among the conditions investigated, the 1100–1150 °C range with a 1 h holding time provides the clearest environmental upgrading and supports consideration of the treated fines as candidate secondary raw-material precursors. Long-term durability, industrial feasibility, off-gas management, and end-use performance remain to be established.

1. Introduction

Municipal solid waste incineration (MSWI) is an integrated component of waste-management systems in industrialised countries because it reduces the volume and mass of residual waste while enabling energy recovery and, increasingly, material recovery from solid residues. Thermal treatment of municipal waste generates bottom ash (BA) from grate furnace burning and fly ash (FA) from air-pollution-control residues (APC), which together account for approximately 20–30 wt% of the input waste (Blasenbauer et al., 2020; Funari et al., 2024; Liu et al., 2015). Among these residues, MSWI bottom ash is generally classified as non-hazardous waste, EWC 19 01 12, and is widely regarded as the most promising stream for material recovery because of its relatively high mineral content and potential use as a secondary raw material in construction-related applications (Alam et al., 2019; Bayuseno & Schmahl, 2010; Chen et al., 2023; Cheng et al., 2024). However, its reuse remains constrained by the mobility of soluble salts and potentially toxic elements. The environmental behaviour of MSWI-BA cannot

* Corresponding author.
E-mail address: luciana.mantovani@unipr.it (L. Mantovani).

https://doi.org/10.1016/j.wasman.2026.115865
Received 26 June 2026; Received in revised form 15 August 2026; Accepted 7 September 2026
Available online 15 September 2026
0956-053X/© 2026 The Authors. Published by Elsevier Ltd. This is an open access article under the CC BY license (http://creativecommons.org/licenses/by/4.0/).

be predicted from bulk chemical composition alone. Bottom ash consists of a heterogeneous assemblage of glass, ceramics, minerals, metallic particles, unburned residues, and secondary weathering products. Consequently, leaching behaviour depends on the mineralogical hosts of contaminants, the degree of weathering and carbonation, the occurrence of soluble chloride- and sulfate-bearing phases, and the accessibility of reactive phases through the pore network and microstructure (Loginova et al., 2023; Luo et al., 2019; Mantovani et al., 2023; Sepúlveda Olea et al., 2024). Recent studies have further shown that trace-element mobility is strongly controlled by mineralogical phase association and pH-dependent processes, highlighting the need for phase-resolved characterization when assessing reuse scenarios (Simon & Scholz, 2024).

Particle size is a key factor controlling both the environmental and technological behaviour of MSWI-BA. Fine fractions are commonly enriched in soluble salts, hydrated Ca-bearing phases, metallic Al residues, sulfates, chlorides, and selected trace elements, whereas coarser fractions are often dominated by glassy, ceramic, and mineral fragments that dilute mobile species (De Matteis et al., 2023; Destefanis et al., 2020; Huber, 2020; Huber et al., 2019, 2020; Mantovani et al., 2021, 2023). Because of their high specific surface area, high reactivity, and abundance of secondary and easily leachable phases, fine fractions often dominate the leaching response of the bulk material under standardized conditions. Different grain-size fractions of MSWI-BA should therefore be considered distinct material streams whose reuse potential depends on their specific chemistry and mineralogy.

Several treatment strategies have been investigated to improve the reuse potential of MSWI-BA, including washing, ageing, carbonation, and mechanical separation (Chen et al., 2025; Destefanis et al., 2020; Santos et al., 2013; Singh et al., 2022; Sun et al., 2024; Vateva et al., 2025).

Washing efficiently removes soluble salts but generates an aqueous residue stream and does not reconstruct the mineral hosts of contaminants; ageing and carbonation require less energy, but their effectiveness is pH-, element-, and time-dependent; mechanical separation recovers metals while leaving a reactive fine fraction.

High-temperature processing should not be regarded as universally superior to these lower-temperature routes, but as a potentially complementary option when phase reconstruction, densification, and partial vitrification are required. By contrast, sintering and vitrification can promote dehydration, dehydroxylation, decarbonation, recrystallization, pore closure, partial melting, and the formation of glassy or glass–ceramic matrices (Rawlings et al., 2006; Stabile et al., 2019). These transformations may reduce contaminant mobility by redistributing elements into newly formed crystalline phases and/or a silicate glass network. In practice, thermal treatment is therefore most plausibly positioned after metal recovery and, where appropriate, washing or carbonation, and applied selectively to the problematic fine fraction.

Recent studies, including Mantovani et al. (2023) and De Matteis et al. (2023), established that the chemical composition, mineralogical hosts, amorphous fraction, and leaching behaviour of fresh MSWI-BA vary with particle size. However, they did not resolve the temperature-dependent sequence from dehydration and recrystallization to liquid-phase sintering and partial vitrification, nor systematically relate these transformations to short-term contaminant release. The remaining gap is therefore mechanistic: it concerns how the non-monotonic evolution of the amorphous fraction, microstructural densification, and element redistribution among mineral and glassy hosts influence the leaching behaviour of thermally treated fine-grained MSWI-BA.

In this context, the present study investigates the 0–2 mm fraction of MSWI bottom ash from the Parma Waste-to-Energy plant, together with selected finer sub-fractions, before and after thermal treatment up to 1200 °C. The novelty lies in the integrated application of XRD quantitative phase analysis, Raman spectroscopy, SEM-EDS, and EN 12457–2 leaching across three grain-size fractions and, for BA1, a high-temperature interval sampled at 25 °C increments. This approach identifies the transition from intermediate-temperature recrystallization to renewed glass formation and incipient liquid-phase sintering above approximately 1050–1100 °C and relates it to the reduction in short-term contaminant release. The objectives are therefore to (i) identify the phase and microstructural transitions controlling the short-term leaching response; (ii) define, for this ash and the fixed heating schedule, the temperature interval providing the most coherent mineralogical, microstructural, and environmental improvement; and (iii) assess the potential and limitations of the treated fines as candidate secondary raw-material precursors.

2. Materials and methods

2.1. Feedstock and sampling

Municipal solid waste incineration bottom ash (MSWI-BA) was collected from the Parma waste-to-energy (WtE) facility, operated by IREN S.p.A. The plant treats municipal solid waste and non-hazardous special waste in a grate-furnace system followed by water quenching. After discharge into a water bath, the ash undergoes short in-plant ageing to reduce the mobility of readily soluble fractions through carbonation with the formation of a leaching-resistant cement onto particle surfaces (Vasarevičius et al., 2022). The nominal treatment capacity of the plant is up to 195,000 t $y^{-}1$, and the annual production of bottom ash is approximately 32,000 t $y^{-}1$, besides recoverable ferrous and non-ferrous metals and FA shares.

In September 2023, sampling was carried out from an outdoor BA stockpile approximately 2–3 m high by multiple increments from different heights and positions of the stockpile, to achieve a composite sample of about 13 kg. The sample was oven-dried at 40 °C to constant mass, riffle-split, quartered, and dry-sieved in accordance with ASTM C136-06. The cumulative particle-size distribution is reported in Fig. S1 and is consistent with previous surveys from the same facility, indicating substantial granulometric stability of the BA stream over time (Mantovani et al., 2021, 2023). The 0–2 mm fraction was selected for detailed characterization and thermal treatment.

The bulk 0–2 mm fraction was further separated into selected finer sub-fractions for thermal-treatment experiments. In particular, the 0–0.2 mm and 0.2–0.5 mm fractions were obtained by dry sieving and used to evaluate the effect of particle size on high-temperature phase evolution and leaching behaviour. Bulk samples of 0–2 mm, 0–0.2 mm, 0.2–0.5 mm fractions are named BA1, BA2, and BA3, respectively (Table 1).

2.2. Thermal treatment

Thermal treatment was performed on BA1, BA2, and BA3. For the BA1 series, sub-samples were placed in ceramic crucibles and heated in an electric kiln (Nannetti GR-20) equipped with six independent chambers. Target temperatures ranged from 100 to 1200 °C. A 100 °C interval was adopted up to 1000 °C, whereas a narrower 25 °C interval was used between 1000 and 1200 °C to resolve the transition from solid-state recrystallization to liquid-phase sintering and partial vitrification. An untreated room-temperature sample was used as the reference.

BA2 and BA3 were treated at temperatures from 650 to 1200 °C using a 50 °C step. These finer fractions were investigated over the selected temperature range to determine whether particle size changed the transition from refractory phase destabilization and recrystallization to sintering and partial vitrification.

All temperature treatments (Table 1) were performed in air using 2 g of material uniaxially pressed into pellets of approximately 10 mm diameter. The furnace was heated at a nominal rate of approximately 2 °C min^{-1} up to the selected target temperature, held at peak temperature for 1 h, and then cooled inside the furnace to near-ambient temperature. The heating rate and 1 h holding time were kept constant

Table 1
Specimen codes, grain-size fractions, and thermal-treatment schedules used in this work.

sample name	grain size (mm)	weight (g)	thermal treatment T (°C)	Time (h)	sample name	grain size (mm)	weight (g)	thermal treatment T (°C)	Time (h)	sample name	grain size (mm)	weight (g)	thermal treatment T (°C)	Time (h)
BA1	**0–2**	**2**	**RT**	/	**BA2**	**0–0.2**	**2**	**RT**	/	**BA3**	**0.2–0.5**	**2**	**RT**	/
			200	1				650	1				650	1
			400	1				700	1				700	1
			600	1				750	1				750	1
			800	1				800	1				800	1
			1000	1				850	1				850	1
			1025	1				900	1				900	1
			1050	1				950	1				950	1
			1075	1				1000	1				1000	1
			1100	1				1050	1				1050	1
			1125	1				1100	1				1100	1
			1150	1				1150	1				1150	1
			1200	1				1200	1				1200	1

throughout the study; consequently, the experiment resolves the effect of temperature but does not optimize residence time or heating rate. Ceramic crucibles were pre-conditioned at 1000 °C for 2 h before use. One crucible was used for each specimen to minimize cross-contamination. Crucibles and specimens were weighed before and after firing to determine mass change; this measurement does not constitute an element-specific volatilization balance.

2.3. Determination of chemical elements in solid samples and leachates

Major elemental oxides were determined by wavelength-dispersive X-ray fluorescence (WD-XRF), whereas selected minor and trace elements were also determined by inductively coupled plasma mass spectrometry (ICP-MS). Major-element oxides were measured by XRF on glass beads prepared by lithium tetraborate fusion. Loss on ignition (LOI) was determined gravimetrically after heating at 950 °C for 2 h. XRF concentrations of selected minor and trace elements are also reported. For ICP-MS analysis, approximately 0.1 g of powdered sample was digested in closed vessels using an HNO_3–HCl–HF mixture. Residual HF was complexed with H_3BO_3 before dilution to 50 ml. Analyses were performed using a Thermo Fisher iCAP-TQe ICP-MS. Elemental determination was based on a calibration with standard solutions of each analyte (Ba, Cr, Cu, Ni, Pb, Sb, and Zn) and checked using indium and rhodium as internal standards. Similarly, ICP-MS was used to determine the aforementioned elements in the leachates. Chloride and sulfate concentrations were determined by ion chromatography using a Metrohm 883 Basic IC Plus equipped with a 20 µL injection loop. A carbonate eluent was used for anion analysis and methanesulfonic acid for cation analysis. Quantification was based on a seven-point calibration for each analyte standard.

2.4. X-ray diffraction and quantitative phase analysis

Powder X-ray diffraction (XRD) data were collected using a Bruker D2 Phaser diffractometer operating in Bragg–Brentano θ–θ geometry with a Cu Kα radiation of $\lambda = 1.54178$ Å at 30 kV and 10 mA. Patterns were recorded over the 5–80° 2θ range using a step size of 0.018° and a counting time of 1 s per step. Samples were spun at 30 rpm during acquisition to improve particle statistics.

Qualitative phase identification was performed with DIFFRAC.EVA v3.1 using the Crystallography Open Database (COD), followed by manual verification to remove duplicate or poorly constrained phase assignments. Quantitative phase analysis (QPA) was carried out by Rietveld refinement using GSAS-II (Toby and Von Dreele, 2013). Refined parameters included phase scale factors, unit-cell parameters, zero shift, and peak-shape coefficients, whereas the background was modelled using a 10-term Chebyshev polynomial.

For all samples included in the temperature-dependent QPA dataset, the amorphous/glassy fraction was estimated using the RIR–Rietveld method with 10 wt% high-purity crystalline Si powder as an internal standard (Gualtieri, 2000; Toby & Von Dreele, 2013). The internal standard was added to finely ground powders and homogenized before XRD acquisition. QPA results were normalized to 100 wt%, including both crystalline and amorphous components. Attention was paid to the temperature-dependent evolution of carbonate-, sulfate-, and chloride-bearing phases and newly formed Ca-silicate phases.

2.5. SEM-EDS and Raman spectroscopy

Raw and thermally treated BA1 samples (0–2 mm fraction) were embedded in epoxy resin and polished to a 1 µm finish, and carbon-coated with an approximately 10 nm conductive layer prior to analysis. Imaging and microanalysis were performed using a JEOL JSM-6400 Scanning Electron Microscope (SEM) equipped with an Oxford Energy-Dispersive Spectroscopy (EDS) system. Typical operating conditions were 20 kV accelerating voltage, approximately 10 mm working distance, and 75 s live time per spectrum. Probe current was adjusted to maintain detector dead time in the 25–35 % range.

Backscattered-electron (BSE) imaging was used to investigate textural and compositional heterogeneity, including glassy domains, relic mineral and ceramic fragments, metallic particles, secondary phases, pores, and newly formed high-temperature crystalline phases. Semi-quantitative chemical composition was estimated with EDS using ZAF correction and manufacturer-provided standards. Elemental maps were acquired on selected areas to document the spatial distribution of chemical elements among crystalline and glassy domains. At least 15 spot analyses were collected for each sample across multiple microstructural domains.

Raman analyses were performed on the same polished sections to support the interpretation of the phase transformations observed by SEM-EDS and XRD. Attention was paid to the evolution of silicate bands within high-temperature products, as these provide information on recrystallization, structural reorganization of the silicate network, and the onset of partial vitrification.

Micro-Raman spectra were acquired on the same embedded samples using a Horiba LabRAM confocal spectrometer coupled to an Olympus BX40 microscope and equipped with a 473 nm diode-pumped solid-state laser. Spectra were collected over the 100–2000 cm^{-1} range with a spectral resolution of approximately 4 cm^{-1}. Instrument calibration was verified before each analytical session using the 520.6 cm^{-1} band of silicon.

Analyses were typically performed with a 100 × objective,

corresponding to a spatial resolution of approximately 2 μm. For each analytical spot, spectra were acquired for 30 s and averaged over at least four accumulations. Data processing was performed using LabSpec 5 by polynomial baseline subtraction.

2.6. Leaching tests and data treatment

The leaching behaviour of raw and thermally treated BA samples was evaluated using a procedure based on EN 12457–2. Since the investigated materials consisted of selected grain size fractions (BA1, BA2 and BA3), no additional crushing was required to meet the < 4 mm particle-size requirement of the standard. Batch leaching tests were performed in deionized water at a liquid-to-solid ratio (L/S) of 10 l $kg^{-}1$ for 24 h. Contact was carried out in acid-washed PE bottles under end-over-end agitation at 10 ± 2 rpm and 20 ± 2 °C. After 24 h, the suspensions were filtered through pre-rinsed 0.45 μm PES membranes.

Sample aliquots for elemental analysis were acidified with conc. HNO_3 and stored at 4 °C, whereas aliquots for anion determination were kept unacidified. Eluate pH, electrical conductivity, and temperature were measured immediately after filtration using a Hanna HI2211 multiparameter instrument.

Minor and trace elements were determined by ICP-MS and ionic species by IC, as described above. Because of the available material, leaching tests were performed in duplicate and not triplicates. Leaching results are reported in mg l^{-1} and compared to appropriate regulatory thresholds (Italian Decree D.Lgs. 121/2020 for eluates after water leaching at L/S = 10 l·kg^{-1}). Procedural blanks and calibration standards were included in each analytical batch. Normalized concentration-to-limit ratios were calculated as C_i/L_i, where C_i is the measured concentration of constituent i in the eluate and L_i is the corresponding regulatory limit. The three temperature series represent predetermined treatment endpoints rather than independent ash populations, and the duplicate leaching measurements provide analytical replication rather than independent treatment replication. Moreover, the XRD phase proportions are compositional data constrained to sum to 100 wt%. These features, together with the limited number of paired leaching endpoints, preclude robust multivariate inference without overfitting. Mineralogy–leaching relationships are therefore interpreted as exploratory associations supported by convergence among XRD-QPA, Raman, SEM-EDS, and leaching trends, rather than as statistically demonstrated causal relationships.

3. Results and discussion

3.1. Chemical and mineralogical behaviour of fine-grained, fresh BA

Table 2 compares XRF data of available BA (size fractions below 2 mm) collected in the 2023 campaign and previous investigation at the same facility (De Matteis et al., 2023; Mantovani et al., 2021, 2023). In all samples, the material is dominated by SiO_2, CaO, Al_2O_3, and Fe_2O_3, whose combined abundance ranges 69–74 wt%. This indicates broad compositional consistency within the Parma stream across the sampled campaigns, but it does not demonstrate inter-plant reproducibility.

Compared with the 2021 fine fraction, the BA1, BA2, and BA3 samples collected in 2023 show show slightly higher SiO_2 and Al_2O_3 contents and lower CaO and LOI value, suggesting a greater contribution from siliceous and aluminosilicate components and a lower carbonate contribution. By contrast, Na_2O, K_2O, Cl, and S are higher in the 2023 samples, indicating a stronger contribution from alkali-rich chloride- and sulfate-bearing components.

Trace elements of environmental concern, including Cu, Zn, Pb, Ni, and Cr, are of the same order of magnitude as those measured in previous samples from the same plant (Table 2) and within the broad compositional range reported for MSWI bottom ash (Funari et al., 2024). However, their environmental relevance depends not only on total concentration in the bulk sample, but also on other sample characteristics such as particle size, chemical speciation, and mineralogical assemblage (Huber et al., 2019, 2020; Sepúlveda Olea et al., 2024; Simon & Scholz, 2024).

Table 2
Elemental composition of BA fine fractions from the 2021 (Mantovani et al. 2023; De Matteis et al. 2023) and 2023 sampling campaigns, grouped according to particle size.

	2021 sampling		*2023 sampling – this work*		
	Mantovani et al. 2023	*De matteis et al. 2024*	*BA1*	*BA2*	*BA3*
	(0–1 mm)	*(0.5–1 mm)*	*(0–2 mm)*	*(0–0.2)*	*(0.2–0.5)*
major elements (wt%)					
SiO_2	28.5	29.2	34.57	29.7	31.4
TiO_2	0.9	0.92	1.09	3.1	1.09
Al_2O_3	8.9	8.96	13.29	10.45	11.29
Fe_2O_3	3.1	3.48	4.71	4.1	3.6
MnO	0.1	0.1	0.11	0.05	0.06
MgO	3.6	3.59	3.51	2.89	3.51
CaO	28.3	28.41	21.72	26.4	24.5
Na2O	2.2	2.18	3.13	4.1	3.06
K_2O	1.3	1.29	1.73	2.1	1.73
P_2O_5	2	2.19	1.83	2.2	1.7
LOI	21.1	19.69	11.68	20.1	18.2
minor and trace elements (ppm)					
As	58	56	8	45	41
Ba	1633	1618	664	1246	1249
Br	11	18	30	12	14
Ce	42	36	51	31	33
Cl	10,204	10,120	12,789	14,340	14,786
Co	50	57	8	14.8	15.1
Cr	639	697	489	650	634
Cu	1700	1885	830	1840	1965
Ga	14	14	5	5	7
Hf	3	<3	<3	<3	<3
La	19	21	30	15	19
Mo	14	13	20.0	19.2	15
Nb	11	10	<3	<3	<3
Nd	14	20	<3	<3	<3
Ni	154	179	177	177	198
Pb	890.7	802	888	888	881
Rb	27.5	27	4	15.6	14
S	14931.7	14,780	23,375	22,658	22,569
Sb	<3	<3	<3	<3	<3
Sc	12.5	13	<3	<3	<3
Se	<3	<3	<3	<3	<3
Sn	55	43	68	59	61
Sr	535	517	434	412	530
Th	7.8	7	10	9	7
U	<3	<3	<3	<3	<3
V	81	79	42	94	81
Y	14	14	<3	<3	<3
Zn	5893	5750	5360	5360	5299
Zr	165	169	33	111	121

BA1 sample (0–2 mm fraction) is relatively enriched in SiO_2 and Al_2O_3, whereas BA2 (0–0.2 mm) and BA3 (0.2–0.5 mm) samples contain higher total alkali contents and LOI values. LOI is higher in the finer BA2 and BA3 fractions than in the bulk BA1 fraction (11.68 % in BA1, 20.1 % in BA2, and 18.2 % in BA3), indicating a greater abundance of carbonate-, sulfate-, and hydrated phases in the finer grain-size classes. The Ca/Si ratio is also higher in BA2 and BA3 than in BA1, particularly in BA2, suggesting a greater contribution from carbonates relative to aluminosilicates.

This trend is consistent with particle-size-resolved studies showing that finer MSWI-BA fractions are commonly enriched in Ca-bearing secondary phases and reactive components, whereas coarser fractions contain a larger proportion of siliceous, glassy, and ceramic particles (Cheng et al., 2024; Marco-Gibert et al., 2026; Sun et al., 2024). Chlorine and sulfur are particularly relevant because they may limit the direct reuse of BA in the construction sector due to corrosion, expansion, and efflorescence issues. In MSWI-BA, our particle-size-resolved data indicate that Cl increases towards the finer fractions, whereas S remains

comparatively stable. Therefore, chloride-bearing phases play an important role in the MSWI-BA mineralogical assemblage, especially in the finest grain-size fractions.

The distribution of trace elements is assessed by enrichment factors relative to the Upper Continental Crust averages as in previous works (Funari et al., 2015). Enrichment factors show that BA1 is enriched in Cu, V, and Ba, and BA2 and BA3 in Cr. Pb and Zn are stable. These results indicate that the environmental assessment of BA fines should rely on particle size analysis and empirical observations of elemental distribution in mineral, amorphous, metallic, and secondary hosts.

XRD-QPA results (Table 3) show that both the previously studied samples and the 2023 ones are dominated by an amorphous to glassy component, accounting for 65–70 wt% of the material. This agrees with earlier studies that previously recognised the relevance of the glassy nature of MSWI-BA (Alam et al., 2019; Bayuseno and Schmahl, 2010). The crystalline assemblage includes calcite, AFm-type phases represented by hydrocalumite-group compounds, ettringite, melilite, feldspar, quartz, minor amounts of portlandite, and Fe oxides or spinels. Vaterite was detected only in the 2021 samples and in earlier samples from other WtE plants in the same Italian region (Funari et al., 2024).

Overall, the phase assemblage remains broadly similar among the available campaigns from the Parma plant, indicating that its principal Ca–Al–silicate framework was relatively consistent over the sampled period. Differences mainly concern the abundance of secondary weathering products. Among the grain-size fractions sampled in 2023, BA1 contains the highest amorphous fraction and larnite (Ca_2SiO_4) content, whereas BA2 and BA3 show slightly lower amorphous contents and higher proportions of calcite, AFm/AFt phases, and hydroxyapatite. These mineralogical differences are consistent with the chemical data and confirm that the finer fractions are enriched in carbonate-, sulfate-, chloride-, and phosphate-bearing phases.

From the viewpoint of thermal treatment, this initial phase assemblage is particularly important. Hydrated phases, carbonates, sulfates, chlorides, and other secondary phases are likely to undergo dehydration, dehydroxylation, decarbonation, and salt release during the early stages of heating. Their preferential concentration in the finer fractions may therefore influence the subsequent evolution of microstructure, phase assemblage, and leaching behaviour. The leaching results for the untreated materials (Table 4) show that their environmental behaviour is more critical than suggested by total chemistry of bulk samples alone. When compared with the Italian acceptance limits for inert and non-hazardous waste, none of the untreated fractions complies with the inert-waste criteria, and each fraction shows at least one measurand exceeding the non-hazardous-waste limit.

In BA1, the main exceedances concern Cr, Sb, Cl^-, and SO_4^{2-}, with Cr and Cl^- exceeding the non-hazardous-waste limits. BA2 is potentially contaminated by Zn and SO_4^{2-}, exceeding the non-hazardous-waste limit. BA3 shows relatively high releases of Cu, Pb, Cl^-, and SO_4^{2-}, with Cu surpassing the non-hazardous-waste limit. BA1 shows the highest release of Cr and Cl^-, possibly reflecting the occurrence of mobile Cr-bearing species and highly soluble chloride carriers in the bulk 0–2 mm fraction. BA2 is characterized by the highest release of Ba, Ni, Zn, and SO_4^{2-}, suggesting preferential mobilization of sulfate-associated and Zn-bearing components in the ultrafine material. BA3 displays the highest Cu and Pb release. Grain-size effects are evident but non-monotonic, indicating that leaching is controlled by element-specific phase distribution rather than by particle size alone, in agreement with recent studies (Sepúlveda Olea et al., 2024; Simon & Scholz, 2024). These results demonstrate that untreated BA fines should be carefully checked for environmental compliance.

3.2. Mineralogy of MSWI BA as a function of temperature

The thermal-treatment experiments were designed to identify, within the tested laboratory conditions, the temperature range in which the short-term leachability of MSWI-BA fines decreases while a sintered/glass–ceramic assemblage develops. Ex situ XRD-QPA data for BA1, BA2, and BA3 were combined with selected Raman spectra and SEM-EDS observations to reconstruct the transformation pathway of the fired products. This combined approach resolves intermediate stages of phase destabilization, recrystallization, sintering, and vitrification; it does not by itself demonstrate long-term environmental stability or product-scale performance.

The untreated materials provide the starting point of quenched MSWI-BA after minimal in-plant ageing. All samples are dominated by an amorphous or poorly crystalline component, followed by hydrated phases and other secondary phases rich in carbonate, sulfate, and chloride (Fig. 1; Table S1). Although these secondary phases are less abundant than the amorphous component, they are relevant in elemental leaching, because they potentially host leachable elements at significant concentrations. Thermal treatment may therefore produce a structurally reorganized high-temperature material with different intermediate- and long-term weathering behaviour. The first transformation regime extends from room temperature to approximately 600 °C. In this interval, AFm/AFt phases and portlandite progressively disappear, whereas becomes relatively more abundant as calcite begins to decrease. This stage mainly corresponds to dehydration, dehydroxylation, and destabilization of low-temperature secondary phases.

Table 3
XRD–QPA results for BA fines from the 2021 and 2023 campaigns, expressed in wt.%. The estimated uncertainty is approximately ± 2 wt%; * indicates the doubtful presence of a minor phase (<1 wt%).

Mineral phase	Chemical formula	*2021 sampling*		*2023 sampling –this work*		
		Mantovani et al. 2023 *(0–1 mm)*	De Matteis et al. 2024 *(0.5–1 mm)*	*BA1 (0–2 mm)*	*BA2 (0–0.2)*	*BA3 (0.2–0.5)*
Hydrocalumite	$Ca_4Al_2(OH)_{12}(Cl,CO_3,OH)_2{\cdot}4H_2O$	3	3	2	2	1
Ettringite	$Ca_6Al_2(SO_4)_3(OH)_{12}{\cdot}26H_2O$	4	3	1	3	2
Calcite	$CaCO_3$	9	10	7	10	11
vaterite	$CaCO_3$	3	2			
Anhydrite	$CaSO_4$	*	*	2	*	1
Melilite	$(Ca,Na)_2(Mg,Fe,Al,Si)_3O_7$	3	3	2	4	4
Larnite	Ca_2SiO_4	*	*	3	1	1
Feldspar	$(K,Ca,Na)[Al(Al,Si)Si_2O_8]$	3	4	4	3	3
Quartz	SiO_2	4	5	4	5	5
Lazurite	$Na_7Ca(Al_6Si_6O_{24})(SO_4)(S_3){\cdot}H_2O$					
Garnet (andradite)	$Ca_3Fe_2^{3+}(SiO_4)_3$					
Pyroxene	$(Fe,Ca,Mg)Si_2O_6$					
Wollastonite	$CaSiO_3$					
Portlandite	$Ca(OH)_2$	2	1	2	1	2
Hematite/Magnetite	Fe_2O_3 / $Fe^{2+}Fe_2^{3+}O_4$	2	2	*	1	1
Hydroxylapatite	$Ca_5(PO_4)_3(OH)$	*	*	3	5	3
Amorphous	amorphous	67	67	70	65	66

Table 4
Leaching test results (mg L¯1) for BA fine fractions from previous sampling campaigns (Mantovani et al., 2023; De Matteis et al., 2023) and for the three bottom-ash fractions investigated in this study, BA1, BA2, and BA3. Results are compared with the Italian acceptance limits for inert and non-hazardous waste according to D. Lgs. 121/2020. Green shading denotes compliance with both limits, orange shading indicates exceedance of the inert-waste limit, and red shading indicates exceedance of both the inert- and non-hazardous-waste limits.

Leachated elements	Mantovani et al. 2023	De matteis et al. 2023	BA1	BA2	BA3	inert waste	non-hazardous waste
	mg L^{-1}						
As	0.000	0	0.03	0	0.001	0.05	0.2
Ba	0.050	0.07	0.4	2.8	1.1	2	10
Cd	0.000	0.002	0.004	0.001	0.001	0.004	0.1
Cr	0.212	0.3	2.3	0.013	0.03	0.05	1
Cu	0.050	0.23	0.22	0.7	7	0.2	5
Mo	0.000	0.002	0	0	0	0.05	1
Ni	0.008	0.005	0.005	0.09	0.001	0.04	1
Pb	0.004	0.016	0.41	0.49	0.56	0.05	1
Sb	0.000	0.001	0.029	0.001	0.001	0.006	0.07
Se	0.019	0.09	0.01	0.002	0.01	0.01	0.05
Zn	0.040	0.03	0.047	9	0.001	0.4	5
Cl^-	678.0	356.0	1697.3	588.9	404.8	80	1500
F^-	0.000	0	0.0	0.02	0	1	15
SO_4^{2-}	420.0	658.0	142.5	2298.0	295.0	100	2000

However, the material is not yet structurally stabilized, because neither extensive sintering nor the formation of a dense glass–ceramic matrix has occurred. A second transformation regime develops between approximately 700 and 950 °C. In this interval, the ash undergoes a marked recrystallization. Melilite and larnite become dominant minerals, whereas quartz and feldspar persist as subordinate relic phases. The decrease in the amorphous or poorly crystalline component indicates that the original disordered matrix is consumed during the formation of new crystalline phases. This behaviour suggests that thermal treatment does not produce an increase in vitrification. Instead, the system passes through an intermediate crystallization stage in which the initial heterogeneous assemblage is reorganized into Ca-rich silicate and aluminosilicate phases.

BA2 and BA3 follow the same general transformation pathway as BA1, with different relative proportions of pyroxene, wollastonite, feldspathoid phases, spinel-group phases, and amorphous material. These differences are consistent with their finer grain size and different abundances of alkalis, Fe, and Al. The finer fractions therefore do not exhibit a separate transformation mechanism; rather, they reach recrystallization and partial vitrification with different phase proportions. The most significant transition occurs above approximately 1000 °C. In this interval, pyroxene and wollastonite become dominant crystalline phases, together with subordinate garnet and Na–Al–Si–S/Cl-bearing phases assignable to sodalite-group feldspathoids. Importantly, the amorphous component increases again above approximately 1050–1100 °C, especially in the finer fractions. This non-monotonic trend marks a transition from a recrystallization-dominated regime to partial melting and vitrification. The high-temperature amorphous/glassy component is therefore interpreted as newly formed glass rather than solely as persistence of the original disordered matrix.

The high-temperature transition is relevant to material upgrading because it produces a candidate glass–ceramic precursor with lower short-term leachability. The glass-bearing matrix and newly formed Ca-silicate phases, including pyroxene and wollastonite, can reduce solution access and redistribute elements among crystalline and amorphous hosts.

The microstructural observations reported in Fig. 2 locate this transition more precisely. Between 1000 and 1075 °C, the fired specimens remain largely granular: densification, pore reduction, and neck growth are visible, but the texture remains characteristic of solid-state sintering. At approximately 1100 °C, much of the granular framework persists. The clearest change occurs between 1125 and 1150 °C, when vesicles and glassy patches develop along grain boundaries and the matrix becomes smoother and more homogeneous, indicating incipient liquid-phase sintering. At 1200 °C, a continuous melt layer at the specimen rim confirms entry into a melt-dominated regime. Together with XRD-QPA and leaching results, this evidence identifies 1100–1150 °C as the most effective tested transition window: it captures partial vitrification and lower short-term release without requiring the more extensive melting observed at 1200 °C. Because heating rate and the 1 h holding time were not varied, process optimization within this interval will require experiments with shorter residence times and different ramps.

SEM-EDS analyses of the 1200 °C products show that this transformation is accompanied by pronounced chemical partitioning among distinct mineral and glassy hosts. Fe, Mg, and Ca are preferentially incorporated into acicular or prismatic Ca–Mg–Fe silicate crystals, whereas Si, Al, Na, and K are mainly retained in the residual aluminosilicate glass. Cr occurs in small clusters enriched in Cr, Mn, and Fe, compatible with spinel-group phases. Sulfur is not uniformly dispersed in the glassy matrices, but it is concentrated in discrete Na–Al-rich domains, indicating the persistence or crystallization of sulfate-bearing feldspathoid phases within the high-temperature assemblage (Fig. 3).

Micro-Raman analyses performed on polished sections at the same microstructural positions investigated by SEM-EDS supported our interpretation further. Owing to the small laser spot size, Raman spectroscopy allowed individual micrometric crystals and inclusions to be analysed directly, overcoming the limitations of bulk XRD in resolving minor and compositionally complex phases. The Ca–Mg–Fe silicate crystals identified by SEM-EDS were confirmed as clinopyroxene-type phases, probably Ti-bearing esseneite. Similarly, the Na–Al–Si–S-rich small crystals were identified as sulfate-bearing feldspathoids, with spectra and XRD patterns consistent with sodalite-group minerals. Raman analytical points also confirmed the occurrence of Cr–Mn–Fe spinel-group microcrystals, which are difficult to resolve by XRD because of their small size and low abundance.

Combined SEM-EDS and Raman show that high-temperature treatment does not simply reduce porosity. Rather, it redistributes environmentally relevant elements into new mineral and glass hosts that differ from those present in the untreated MSWI-BA. Ca, Mg, Fe, and other transition metals are incorporated into newly formed Ca-silicates and spinel-group phases, whereas alkalis and Al remain largely associated with the residual glass and feldspathoid domains. Sulfur is at least partly retained in discrete sulfate-bearing feldspathoids instead of being homogeneously dispersed in the glass. The leaching behaviour of the treated material should therefore be interpreted as the combined result of densification, partial vitrification, and host-phase reorganization. This interpretation is consistent with the influence of glass composition on hazardous-element inertisation in vitrified silicate ceramics reported by Conte et al. (2024).

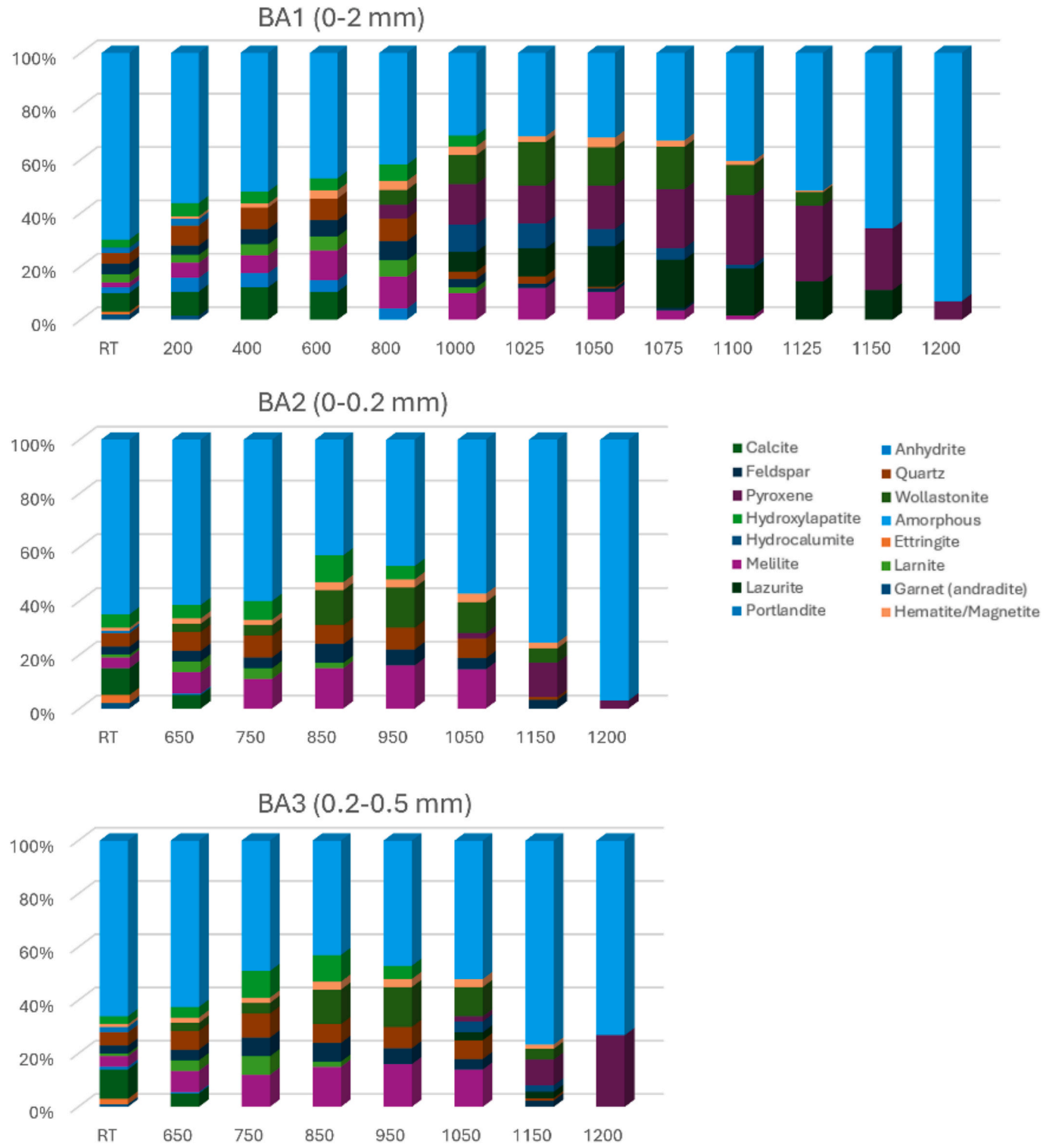


Fig. 1. Temperature-dependent XRD-QPA phase assemblages of the BA1, BA2, and BA3 fractions after thermal treatment. BA1 corresponds to the 0–2 mm fraction, BA2 to the 0–0.2 mm fraction, and BA3 to the 0.2–0.5 mm fraction. The amorphous component includes glassy and poorly crystalline material. Values are normalized to 100 wt%.

3.3. Temperature-dependent leaching behaviour and MSWI-BA upgrading after thermal treatment

The results of leaching experiments indicate that the leaching performance of the treated fractions of MSWI-BA, i.e. BA1, BA2, and BA3, is strongly temperature-dependent and follows the mineralogical and microstructural evolution described above. The improvement is not gradual over the whole heating interval, but it becomes particularly evident once the material enters the high-temperature recrystallization and partial vitrification regime.

Untreated and low-temperature-treated samples are characterized by alkaline pH and high electrical conductivity, consistent with the persistence of reactive Ca-bearing phases, hydrated secondary phases, and readily soluble salts. With increasing temperature, electrical

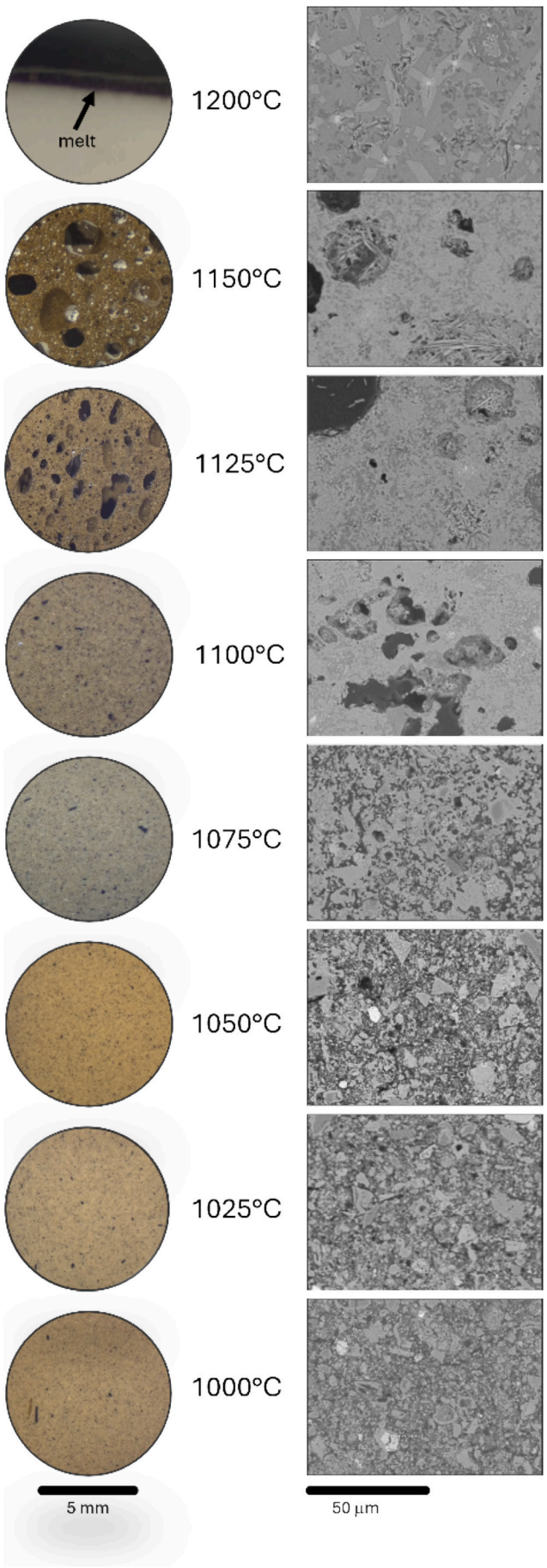


Fig. 2. Stereomicroscope and SEM-BSE images of selected BA1 specimens after thermal treatment, showing the progressive transition from granular sintered textures to partially vitrified products and, at 1200 °C, the development of a melt layer at the specimen rim.

conductivity decreases, particularly above approximately 1000–1050 °C, indicating a lower concentration of ionic species in the eluates. This trend is consistent with destabilization of chloride- and sulfate-bearing phases and with some combination of volatilization, redistribution, and incorporation into less soluble crystalline and glassy hosts. Because neither off-gas/condensate analysis nor element-specific solid mass balances were performed, the relative contributions of volatilization and immobilization cannot be quantified from the present data.

Chloride and sulfate represent the main soluble ions at low temperature. Chloride concentrations are high up to approximately 1075 °C, especially in BA2, and decrease markedly at $\geq$ 1100 °C. This sharp reduction coincides with the temperature interval in which SEM observations indicate liquid-phase sintering and the onset of partial vitrification. Sulfate shows a less regular trend than that of chloride, with pronounced peaks at intermediate temperatures (below 1075° C), especially in BA1, before decreasing at higher temperatures (Fig. 4). This behaviour suggests that sulfate leaching is controlled not only by the progressive breakdown of sulfate-bearing phases, but also by transient redistribution among newly formed Ca-, Na-, and Al-bearing phases during recrystallization. At the highest temperatures, the limited sulfate leaching is consistent with the development of a denser glass–ceramic matrix and with the partial retention of sulfur in discrete sulfate-bearing feldspathoid domains observed by SEM-EDS and Raman spectroscopy.

The normalized concentration-to-limit ratios, C_i/L_i, reported in Fig. 4 for BA1 and BA2, highlight this transition. Values above 1 indicate exceedance of the adopted regulatory limit, whereas values below 1 indicate compliance with the corresponding limit. Regarding chloride, both BA1 and BA2 remain above the limit over much of the low- and intermediate-temperature range. At approximately 1100 °C and above, the concentrations fall below the limit of inert/non-hazardous waste. Sulfate is more variable, but its release also decreases strongly at the highest temperatures, particularly in BA2.

Regarding minor and trace elements, their release does not decrease monotonically with temperature (e.g., Cr and Cu). In BA1, Cr shows a pronounced intermediate-temperature increase before dropping at higher temperature, whereas Cu remains close to or slightly above the limit over part of the low-temperature interval and decreases after high-temperature treatment. BA2 displays elevated Cr release at low-to-intermediate temperatures, followed by a sharp decrease above approximately 1050–1100 °C. Zn is generally less problematic, remaining close to or below the limit in most treated samples.

These trends indicate that the decomposition of secondary phases alone is not sufficient to ensure trace-element stabilization. Instead, the most effective reduction in elemental mobility occurs when recrystallization is accompanied by densification, renewed growth of the amorphous/glassy component, and partial vitrification. The leaching data therefore indicate a transition from salt-dominated leaching at low temperature to matrix-controlled leaching at high temperature. Below approximately 1000 °C, the environmental response is mainly governed by the persistence and destabilization of soluble secondary phases. Above approximately 1100 °C, the sharp decrease in chloride release, the reduction of sulfate mobility, and the lower release of several regulated elements indicate that the fine MSWI-BA has crossed a structural threshold. At this stage, the formation of a denser glass–ceramic matrix, together with newly crystallized Ca-silicates, feldspathoid domains, and spinel-group phases, reduces the accessibility and mobility of leachable components.

Among the conditions investigated, the clearest improvement is observed at 1100–1150 °C with the fixed 1 h holding time and nominal

(caption on next column)

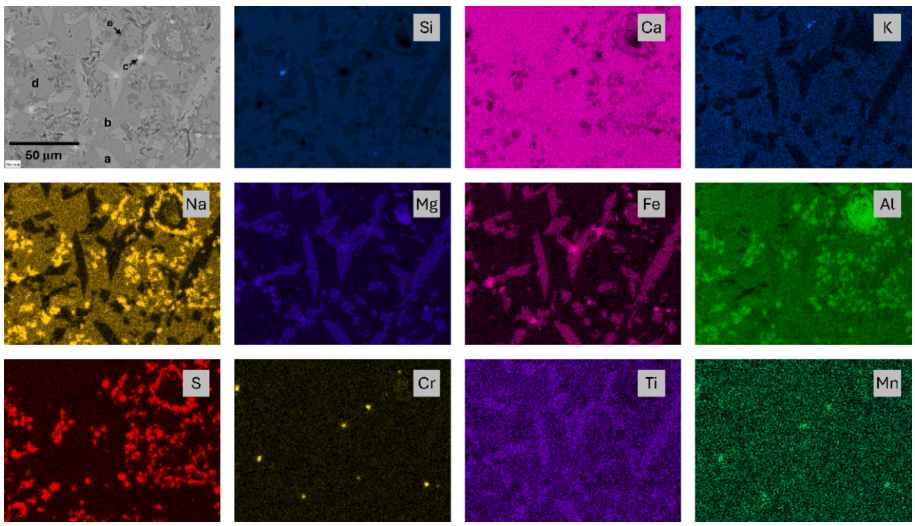


Fig. 3. SEM-BSE image and elemental maps of the BA1 sample treated at 1200 °C, showing the partitioning of major and minor elements among clinopyroxene-type crystals (a,b), Cr–Mn–Fe spinel-group microcrystals (c), residual aluminosilicate glass (d), and Na–Al–S-rich feldspathoid domains (e).

2 °C min^{-1} heating rate. This interval coincides with the onset of liquid-phase sintering and partial vitrification identified by XRD-QPA, SEM-EDS, and Raman spectroscopy. The lower release measured after thermal treatment is therefore associated with mineralogical and microstructural reorganization, but it represents performance in a 24 h EN 12457–2 batch test and should not be interpreted as proof of long-term stability.

3.4. Practical implementation, energy demand, and off-gas control

The experiments used 2 g pressed pellets in a laboratory electric kiln and cannot directly define an industrial process. Potential continuous configurations include rotary, moving-hearth, roller, or slagging/vitrification furnaces, selected according to the desired degree of sintering or melting. Fine BA would probably require controlled feeding or granulation, dust containment, residence-time control, and heat recovery. Chlorine- and sulfur-bearing species and potentially volatile metals may transfer to the gas phase during heating; industrial implementation would therefore require enclosed off-gas handling, rapid cooling where appropriate, particulate filtration, and acid-gas/metal capture, followed by management of the resulting secondary residues. The total mass changes measured here combine dehydration, decarbonation, organic loss, salt release, and possible metal volatilization and cannot quantify any element-specific loss. Off-gas, condensate, furnace-deposit, and residual-solid analyses are needed to close elemental mass balances. This qualification is consistent with the element-dependent volatility reported for MSWI-BA vitrification by Stabile et al. (2019).

Heating fine BA to 1100–1150 °C is energy- and capital-intensive. No process-energy inventory, carbon-footprint calculation, or techno-economic analysis was performed, so practical or financial viability is not claimed. Feasibility will depend on feed moisture, treated mass, throughput, furnace efficiency, preheating, use of waste heat or low-carbon electricity, heat recovery, off-gas-treatment requirements, avoided disposal costs, and the value and substitution credit of the final product. Selective treatment of only the problematic fine fraction, after metal recovery and possibly washing or carbonation, would reduce the mass exposed to high temperature. Comparative life-cycle and techno-economic assessments at pilot scale are nevertheless required to determine whether the environmental and material benefits offset the energy, carbon, and investment burdens.

3.5. Transferability, long-term durability, and end-use qualification

Bottom-ash composition and phase assemblage depend on waste input, furnace type and operating conditions, burnout, cooling and quenching, metal recovery, and ageing. Composite stockpile sampling and comparison with earlier Parma campaigns reduce the influence of local heterogeneity and show broad within-plant consistency, but they do not establish inter-plant generality. The transformation sequence identified here may be transferable to comparable Ca–Si–Al-rich water-quenched grate ashes, whereas the exact transition temperature and leaching response may shift with composition. Multi-season sampling from several WtE plants is therefore necessary before generalizing the 1100–1150 °C window (Mantovani et al., 2023).

The EN 12457–2 test measures release during 24 h contact and does not establish persistence under long-term weathering. Carbonation, hydration, glass alteration, secondary-phase precipitation, wet–dry cycling, and changes in pH and CO_2 exposure may modify release over time. The revised interpretation is therefore limited to lower short-term leachability. Long-term validation should combine accelerated ageing with pH-dependence and percolation tests for granular material and, after a product is formulated, dynamic surface-leaching tests appropriate to monolithic or construction products.

Likewise, densification observed by SEM is not evidence of adequate mechanical performance. No final aggregate, ceramic, or cementitious product was manufactured and no strength or durability tests were conducted. The treated ash is therefore described only as a candidate precursor. Qualification for a specific reuse route will require, as applicable, density, porosity and water absorption, compressive and flexural strength, abrasion or fragmentation resistance, dimensional stability, freeze–thaw and wet–dry durability, and leaching tests on the final product. This need for product-level validation is consistent with studies assessing both the environmental and mechanical performance of concrete containing vitrified MSWI bottom ash (Sirico et al., 2024).

4. Conclusions

This study investigated the thermal treatment of fine MSWI bottom-ash fractions from the Parma Waste-to-Energy plant by linking phase evolution and microstructural reorganization with elemental release in a standardized 24 h batch-leaching test. Untreated fine fractions are environmentally critical because they concentrate soluble salts, secondary Ca-bearing phases, and other leaching-sensitive minerals. Their leaching response cannot be explained by bulk composition alone, but

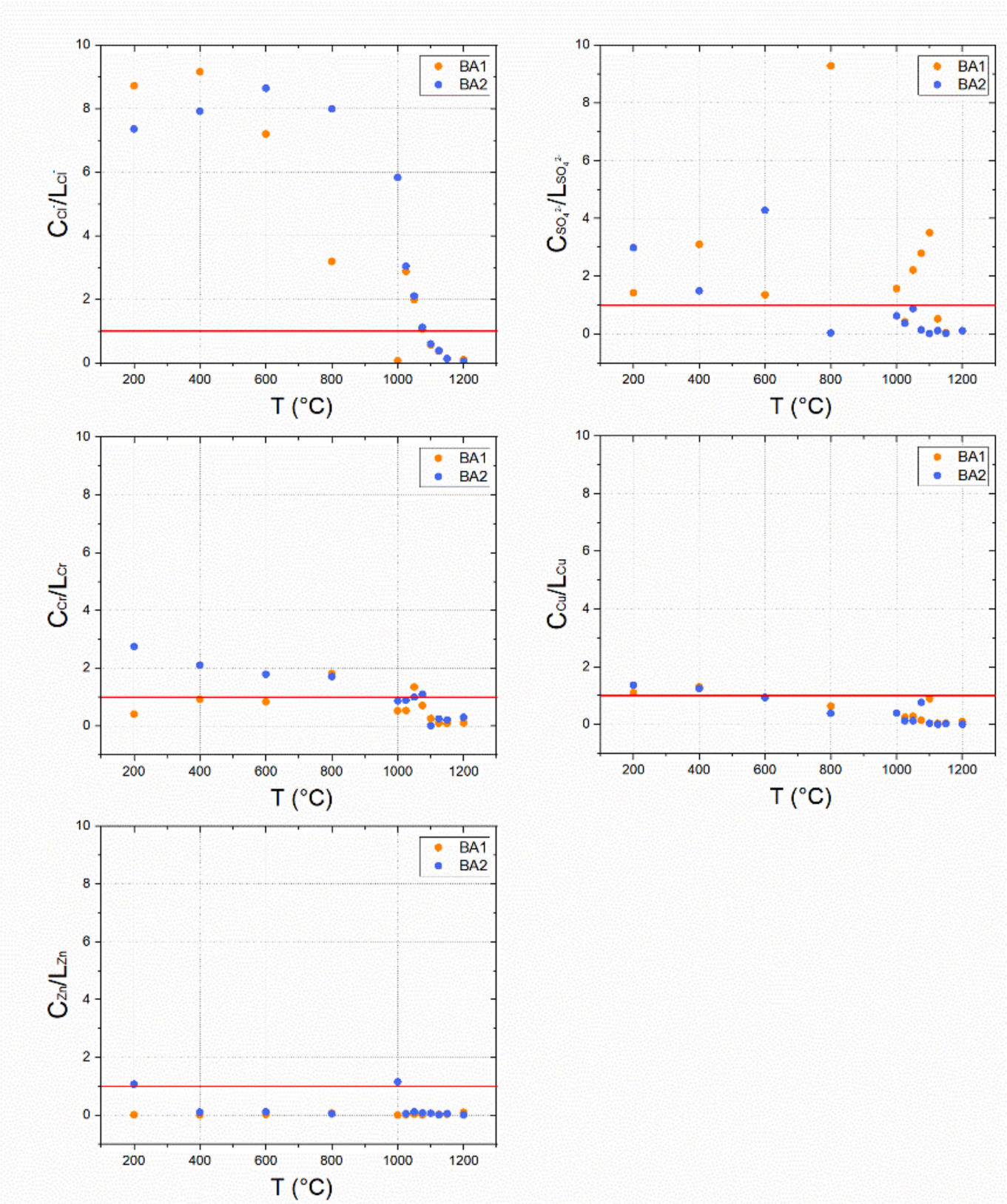


Fig. 4. Normalized leaching response of selected regulated constituents in BA1 and BA2 as a function of thermal-treatment temperature. C_i/L_i represents the ratio between the measured eluate concentration of constituent i and the corresponding adopted regulatory limit. The red horizontal line indicates $C_i/L_i = 1$; values above this line indicate exceedance of the limit, whereas values below this line indicate compliance.

depends on the distribution of potentially toxic elements among amorphous, crystalline, metallic, and secondary mineral hosts. Because the feedstock was collected from one plant, the conclusions directly apply to the investigated Parma ash; they provide mechanistic hypotheses for comparable Ca–Si–Al-rich, water-quenched grate ashes rather than a universal temperature prescription.

Thermal treatment progressively transforms the untreated ash from a heterogeneous assemblage of altered minerals into a sintered and partially vitrified glass–ceramic material. The pathway is non-monotonic: dehydration, dehydroxylation, decarbonation, and recrystallization dominate at low-to-intermediate temperatures, whereas above approximately 1050–1100 °C the amorphous/glassy component increases and liquid-phase sintering begins. Among the tested conditions, the most coherent mineralogical, microstructural, and short-term leaching improvement occurs at 1100–1150 °C with a 1 h hold. SEM-EDS and Raman observations show that this improvement is associated not only with pore reduction but also with redistribution among newly formed Ca-silicates, spinel-group phases, residual aluminosilicate glass, and sulfate-bearing feldspathoid domains. Nevertheless, the present data cannot separate immobilization from element loss by volatilization.

These findings show that the reduction in short-term leachability is associated with identifiable mineralogical and microstructural transformations rather than with heating alone. Further work should include multi-plant and multi-season validation; factorial optimization of temperature, heating rate, and residence time; element-specific mass balances and off-gas capture; pilot-scale continuous processing; long-term weathering and pH-dependent/percolation tests; end-use mechanical qualification; and comparative techno-economic and life-cycle assessment. These steps are required to establish whether selective thermal treatment of MSWI-BA fines is environmentally, energetically, and financially viable at industrial scale.

The data supporting the findings of this study are included in the article and its Supplementary Material.

Declaration of generative AI and AI-assisted technologies.

During the preparation of this work, the authors used OpenAI for language editing and readability improvement. After using this tool, the authors reviewed and edited the content as needed and take full responsibility for the content of the published article.

CRediT authorship contribution statement

Luciana Mantovani: Writing – review & editing, Writing – original draft, Supervision, Methodology, Investigation, Funding acquisition, Data curation, Conceptualization. **Sabrina Nazzareni:** Writing – review & editing, Supervision, Investigation. **Andrea Bernasconi:** Writing – review & editing, Writing – original draft, Supervision, Methodology, Investigation, Formal analysis, Data curation. **Enrico Destefanis:** Writing – review & editing, Writing – original draft, Resources, Methodology, Data curation. **Caterina Caviglia:** Writing – review & editing, Validation, Supervision, Methodology, Investigation. **Chiara De Matteis:** Writing – review & editing, Validation, Supervision, Methodology. **Valerio Funari:** Writing – review & editing, Writing – original draft, Validation, Supervision, Resources, Methodology, Investigation, Funding acquisition, Conceptualization. **Simone Toller:** Writing – review & editing, Validation, Methodology, Investigation. **Laura Fornasini:** Writing – review & editing, Writing – original draft, Supervision, Methodology, Investigation. **Danilo Bersani:** Writing – review & editing, Validation, Supervision, Resources. **Mario Tribaudino:** Writing – review & editing, Writing – original draft, Visualization, Validation, Supervision, Resources, Investigation, Funding acquisition, Conceptualization.

Funding

This research was financially supported by “Research Grant in memory of Prof. Fiorenzo Mazzi of the Italian Society of Mineralogy and Petrology (SIMP).” In addition, this work benefited from the equipment and framework of the COMP-R Initiatives, funded by the “Departments of Excellence” program of the Italian Ministry for University and Research (MUR, 2023–2027).

Declaration of competing interest

The authors declare that they have no known competing financial interests or personal relationships that could have appeared to influence the work reported in this paper.

Acknowledgements

The authors gratefully acknowledge IREN S.p.A. for providing access to the MSWI bottom ash samples and technical information on the Parma waste-to-energy plant. The authors also thank Enrico Maria Selmo, Andrea Comelli, Nadia Curetti and Luca Barchi for their valuable assistance and continuous support during laboratory activities.

Appendix A. Supplementary data

Supplementary data to this article can be found online at https://doi.org/10.1016/j.wasman.2026.115865.

Data availability

Data will be made available on request.

References

Alam, Q., Schollbach, K., van Hoek, C., van der Laan, S., de Wolf, T., Brouwers, H.J.H., 2019. In-depth mineralogical quantification of MSWI bottom ash phases and their association with potentially toxic elements. Waste Manag. 87, 1–12.

Bayuseno, A.P., Schmahl, W.W., 2010. Understanding the chemical and mineralogical properties of the inorganic portion of MSWI bottom ash. Waste Manag. 30 (8–9), 1509–1520. https://doi.org/10.1016/J.WASMAN.2010.03.010.

Blasenbauer, D., Huber, F., Lederer, J., Quina, M.J., Blanc-Biscarat, D., Bogush, A., Bontempi, E., Blondeau, J., Chimenos, J.M., Dahlbo, H., 2020. Legal situation and current practice of waste incineration bottom ash utilisation in Europe. Waste Manag. 102, 868–883.

Chen, B., Perumal, P., Illikainen, M., Ye, G., 2023. A review on the utilization of municipal solid waste incineration (MSWI) bottom ash as a mineral resource for construction materials. Journal of Building Engineering 71, 106386. https://doi.org/10.1016/J.JOBE.2023.106386.

Chen, B., Perumal, P., Liu, C., Chen, Y., Chang, C., Pavlin, M., Kvočka, D., Ducman, V., Luukkonen, T., Illikainen, M., & Ye, G. (2025). Municipal solid waste incineration (MSWI) bottom ash-blended cementitious materials: Performance, challenges, and potential solutions. In *Critical Reviews in Environmental Science and Technology* (Vol. 55, Number 19, pp. 1506–1533). Taylor and Francis Ltd. Doi: 10.1080/10643389.2025.2548287.

Cheng, Y., Gao, G., Chen, L., Du, W., Mu, W., Yan, Y., Sun, H., 2024. Physical and mechanical study of municipal solid waste incineration (MSWI) bottom ash with different particle size distribution. Constr. Build. Mater. 416, 135137. https://doi.org/10.1016/J.CONBUILDMAT.2024.135137.

Conte, S., Molinari, C., Ardit, M., Mantovani, L., Tribaudino, M., Cruciani, G., Dondi, M., Zanelli, C., 2024. Hazardous element inertisation in vitrified silicate ceramics: effect of different matrices. J. Hazard. Mater. 474, 134657. https://doi.org/10.1016/J.JHAZMAT.2024.134657.

De Matteis, C., Mantovani, L., Tribaudino, M., Bernasconi, A., Destefanis, E., Caviglia, C., Toller, S., Dinelli, E., Funari, V., 2023. Sequential extraction procedure of municipal solid waste incineration (MSWI) bottom ash targeting grain size and the amorphous fraction. Front. Environ. Sci. 11. https://doi.org/10.3389/fenvs.2023.1254205.

De Matteis, C., Pollastri, S., Mantovani, L., Tribaudino, M., 2024. Potentially toxic elements speciation in bottom ashes from a municipal solid waste incinerator: A combined SEM-EDS, μ-XRF and μ-XANES study. Environmental Advances 15, 100453.

Destefanis, E., Caviglia, C., Bernasconi, D., Bicchi, E., Boero, R., Bonadiman, C., Confalonieri, G., Corazzari, I., Mandrone, G., Pastero, L., Pavese, A., Turci, F., Wehrung, Q., 2020. Valorization of mswi bottom ash as a function of particle size distribution, using steam washing. Sustainability (switzerland) 12 (22), 1–17. https://doi.org/10.3390/su12229461.

Funari, V., Braga, R., Bokhari, S.N.H., Dinelli, E., Meisel, T., 2015. Solid residues from italian municipal solid waste incinerators: a source for “‘critical’” raw materials. Waste Manag. 45, 206–216. https://doi.org/10.1016/j.wasman.2014.11.005.

Funari, V., Ghani, J., & Mantovani, L. (2024). Resource recovery from municipal solid waste incineration bottom ash. In *Treatment and Utilization of Combustion and*

Incineration Residues (pp. 511–531). Elsevier. Doi: 10.1016/B978-0-12-817491-3.00014-3.

Gualtieri, A.F., 2000. Accuracy of XRPD QPA using the combined Rietveld–RIR method. J. Appl. Cryst. 33 (2), 267–278.

Huber, F., 2020. Modelling of material recovery from waste incineration bottom ash. Waste Manag. 105, 61–72. https://doi.org/10.1016/j.wasman.2020.01.034.

Huber, F., Blasenbauer, D., Aschenbrenner, P., Fellner, J., 2019. Chemical composition and leachability of differently sized material fractions of municipal solid waste incineration bottom ash. Waste Manag. 95, 593–603. https://doi.org/10.1016/j.wasman.2019.06.047.

Huber, F., Blasenbauer, D., Aschenbrenner, P., Fellner, J., 2020. Complete determination of the material composition of municipal solid waste incineration bottom ash. Waste Manag. 102, 677–685. https://doi.org/10.1016/J.WASMAN.2019.11.036.

Liu, A., Ren, F., Lin, W.Y., Wang, J.Y., 2015. A review of municipal solid waste environmental standards with a focus on incinerator residues. Int. J. Sustain. Built Environ. 4 (2), 165–188. https://doi.org/10.1016/J.IJSBE.2015.11.002.

Loginova, E., Schollbach, K., Proskurnin, M., Brouwers, H.J.H., 2023. Mechanical performance and microstructural properties of cement mortars containing MSWI BA as a minor additional constituent. Case Stud. Constr. Mater. 18, e01701. https://doi.org/10.1016/J.CSCM.2022.E01701.

Luo, H., Cheng, Y., He, D., Yang, E.H., 2019. Review of leaching behavior of municipal solid waste incineration (MSWI) ash. Sci. Total Environ. 668, 90–103. https://doi.org/10.1016/j.scitotenv.2019.03.004.

Mantovani, L., Tribaudino, M., Matteis, C.D., Funari, V., 2021. Particle size and potential toxic Element Speciation in Municipal Solid Waste Incineration (MSWI) Bottom Ash. Sustainability 13 (4), 1911. https://doi.org/10.3390/su13041911.

Mantovani, L., De Matteis, C., Tribaudino, M., Boschetti, T., Funari, V., Dinelli, E., Toller, S., Pelagatti, P., 2023. Grain size and mineralogical constraints on leaching in the bottom ashes from municipal solid waste incineration: a comparison of five plants in northern Italy. Front. Environ. Sci. 11. https://doi.org/10.3389/fenvs.2023.1179272.

Marco-Gibert, J., Cuspoca, F., Cordoba, J.C., Pujadó, N., Mañosa, J., Faneca, G., Chimenos, J.M., 2026. Potential use of municipal solid waste incineration bottom ash as supplementary cementitious materials based on particle size fraction. Materials and Structures/materiaux et Constructions 59 (4). https://doi.org/10.1617/s11527-026-03088-3.

Rawlings, R.D., Wu, J.P., Boccaccini, A.R., 2006. Glass-ceramics: their production from wastes-a Review. Journal of Materials Science (vol. 41 (3), 733–761. https://doi.org/10.1007/s10853-06-6554-3.

Santos, R.M., Mertens, G., Salman, M., Cizer, Ö., Van Gerven, T., 2013. Comparative study of ageing, heat treatment and accelerated carbonation for stabilization of municipal solid waste incineration bottom ash in view of reducing regulated heavy metal/metalloid leaching. J. Environ. Manage. 128, 807–821. https://doi.org/10.1016/j.jenvman.2013.06.033.

Sepúlveda Olea, F.E., Burke, I.T., Mohammad, A., Stewart, D.I., 2024. Reuse potential of municipal solid waste incinerator bottom ash as secondary aggregate: Material characteristics, persistent organic pollutant content and effects of pH and selected environmental lixiviants on leaching behaviour. Waste Manag. 187, 262–274. https://doi.org/10.1016/J.WASMAN.2024.07.026.

Simon, F.G., Scholz, P., 2024. Sequential Extraction of Incineration Bottom Ash: Conclusions Regarding Ecotoxicity. Applied Sciences (switzerland) 14 (13). https://doi.org/10.3390/app14135541.

Singh, A., Zhou, Y., Gupta, V., Sharma, R., 2022. Sustainable use of different size fractions of municipal solid waste incinerator bottom ash and recycled fine aggregates in cement mortar. Case Stud. Constr. Mater. 17, e01434. https://doi.org/10.1016/J.CSCM.2022.E01434.

Sirico, A., Bernardi, P., Belletti, B., Sciancalepore, C., Milanese, D., Paini, A., Vignali, G., 2024. Environmental and mechanical analysis of low-carbon concrete with vitrified MSW incineration bottom ash as cement replacement. Struct. Concr. 25 (4), 2968–2990. https://doi.org/10.1002/suco.202300615.

Stabile, P., Bello, M., Petrelli, M., Paris, E., Carroll, M.R., 2019. Vitrification treatment of municipal solid waste bottom ash. Waste Manag. 95, 250–258. https://doi.org/10.1016/J.WASMAN.2019.06.021.

Sun, Y., Chen, B., Zhang, S., Blom, K., Luković, M., Ye, G., 2024. Characterization, pre-treatment, and potential applications of fine MSWI bottom ash as a supplementary cementitious material. Constr. Build. Mater. 421, 135769. https://doi.org/10.1016/J.CONBUILDMAT.2024.135769.

Toby, B.H., Von Dreele, R.B., 2013. GSAS-II: the genesis of a modern open-source all purpose crystallography software package. Applied Crystallography 46 (2), 544–549.

Vasarevičius, S., Seniūnaitė, J., Vaišis, V., 2022. Impact of Natural Weathering on Stabilization of Heavy Metals (Cu, Zn, and Pb) in MSWI Bottom Ash. Applied Sciences (switzerland) 12 (7). https://doi.org/10.3390/app12073419.

Vateva, I., Laabs, M., Middendorf, B., Laner, D., 2025. Treatment of fine and medium fractions of MSWI bottom ash for use in concrete: a German case study. Waste Manag. 198, 117–127. https://doi.org/10.1016/J.WASMAN.2025.02.050.